Effects of unequally biaxial misfit strains on polarization phase diagrams in embedded ferroelectric thin layers: Phase field simulations

Ping-Li Liu,[1,2] Jie Wang,[3] Tong-Yi Zhang,[2,3] Yulan Li,[4] Long-Qing Chen,[4] Xing-Qiao Ma,[5] Wu-Yang Chu,[1] and Li-Jie Qiao[1,a)]

[1]*Corrosion and Protection Center, Key Laboratory of Environmental Fracture, University of Science and Technology Beijing, Beijing 100083, People's Republic of China*

[2]*The Hong Kong-Beijing UST Joint Research Center, HKUST, Fok Ying Tung Graduate School, Nansha, Guangzhou, People's Republic of China*

[3]*Department of Mechanical Engineering, Hong Kong University of Science and Technology, Clear Water Bay, Kowloon, Hong Kong, China*

[4]*Department of Materials Science and Engineering, The Pennsylvania State University, University Park, Pennsylvania 16802, USA*

[5]*Department of Application Physics, University of Science and Technology Beijing, Beijing 100083, People's Republic of China*

(Received 1 July 2008; accepted 31 July 2008; published online 3 October 2008)

Phase field simulations were conducted to investigate the effects of unequally biaxial misfit strains on domain stability diagrams and equilibrium domain structures in an epitaxial ferroelectric $PbTiO_3$ thin layer, which is sandwiched in a nonferroelectric medium. The simulations reveal a multidomain structure in the layer and allow constructing "misfit strain-misfit strain" and "temperature-misfit strain" phase diagrams. It is found that unequally biaxial misfit strains may lead to the presence of a single tetragonal variant, either *a*-domains or *b*-domains, which do not exist if the misfit strains are equally biaxial. © *2008 American Institute of Physics*. [DOI: 10.1063/1.2975161]

Ferroelectric thin films have found wide applications and will find wider applications.[1–5] For a $PbZr_{1-x}Ti_xO_3$(PZT) film, the polarization phase could be drastically modified by a substrate constraint, as it has been shown recently for other systems.[6–13] The misfit strains between a ferroelectric thin film and its substrate are able to change the Curie temperature, the order of the paraelectric/ferroelectric phase transition, the equilibrium polarization states, and the dielectric properties of the material.[8] The "misfit strain-temperature" phase diagrams of ferroelectric thin films have previously been constructed.[8–11] Equally biaxial misfit strains, called the isotropic misfit strains, are induced when ferroelectric thin films are grown on cubic substrates. If a ferroelectric thin film is grown on a tetragonal substrate, unequally biaxial (or anisotropic) misfit strains will be produced, as illustrated by recent experimental studies.[14–16] By thermodynamics calculations, Wang and Zhang[11] theoretically studied the effects of unequally biaxial misfit strains on polarization phases and structure in a single-domain epitaxial ferroelectric thin film. Thermodynamics theory is often used to study the effects of anisotropic strain on phase diagrams.[17–19] Phase-field method is a powerful tool in the study of the domain structures in ferroelectric thin films, especially in three-dimensional simulations.[10,13]

In the present work, we study a ferroelectric thin layer, which is sandwiched in a nonferroelectric material. The sandwiched structure might be fabricated by epitaxially depositing a ferroelectric thin layer on a nonferroelectric substrate and then capping the layer epitaxially with the same material as the substrate. The interfaces between the layer/nonferroelectric medium are coherent. The spontaneous polarization vector $\mathbf{P}=(P_1,P_2,P_3)$ is the primary order parameter, and the temporal domain structure evolution is described by the time-dependent Ginzburg–Laudau (TDGL) equation.

$$\frac{\partial P_i(\mathbf{r},t)}{\partial t} = -L\frac{\delta F}{\delta P_i(\mathbf{r},t)} \quad (i=1,2,3), \tag{1}$$

where L is the kinetic coefficient, F is the total free energy of the system, $\delta F/\delta P_i(\mathbf{r},t)$ represents the thermodynamic driving force for the spatial and temporal evolution of the simulated system, and $\mathbf{r}$ denotes the spatial vector $\mathbf{r}=(x_1,x_2,x_3)$. In this work, we ignore any possible interface contributions to the free energy as discussed in Refs 20 and 21. The total free energy can be expressed as

$$F = \int_V [f_{\text{Lan}}(P_i) + f_{\text{grad}}(\partial P_i/\partial x_j) + f_{\text{elas}}(P_i,\varepsilon_{ij}) + f_{\text{elec}}(E_i,P_i)]dV, \tag{2}$$

in which f_{Lan} is the Landau free energy density, which is given by[22]

$$f_{\text{Lan}}(P_i) = \alpha_1(P_1^2+P_2^2+P_3^2) + \alpha_{11}(P_1^4+P_2^4+P_3^4) + \alpha_{12}(P_1^2P_2^2+P_2^2P_3^2+P_1^2P_3^2) + \alpha_{111}(P_1^6+P_2^6+P_3^6) + \alpha_{112}[(P_1^4(P_2^2+P_3^2)+P_2^4(P_1^2+P_3^2)+P_3^4(P_1^2+P_2^2)] + \alpha_{123}P_1^2P_2^2P_3^2, \tag{3}$$

where α_1 is the dielectric stiffness and α_{11}, α_{12}, α_{111}, α_{112}, and α_{123} are higher order dielectric stiffness coefficients. In Eq. (2), $f_{\text{grad}}=1/2\,g_{ijkl}(\partial P_i/\partial x_j)(\partial P_k/\partial x_l)$ is the gradient energy density, where g_{ijkl} are the gradient energy coefficients.[10,13] $f_{\text{elas}}=1/2\,c_{ijkl}(\varepsilon_{ij}-\varepsilon_{ij}^0)(\varepsilon_{kl}-\varepsilon_{kl}^0)$ denotes the elastic energy density, where c_{ijkl} are the elastic constants, ε_{ij} are the total strains, and ε_{ij}^0 are the spontaneous strains or stress-free strains. In the present work, the layer/substrate

a)Author to whom correspondence should be addressed. FAX: +86 10 6233 2345. Electronic mail: lqiao@ustb.edu.cn.

misfit strains are $e_{11}=\bar{\varepsilon}_{11}$ and $e_{22}=\bar{\varepsilon}_{22}$ along the x_1 and x_2 axes, respectively. The overbar indicates an average over the layer. The spontaneous strains are related to the spontaneous polarization components in the form of $\varepsilon_{ij}^0=Q_{ijkl}P_kP_l$, where Q_{ijkl} are the electrostrictive coefficients. The internal stresses generated by the inhomogeneous spontaneous strains and the misfit strains are $\sigma_{ij}=c_{ijkl}(\varepsilon_{kl}-\varepsilon_{kl}^0)$. The stresses must satisfy the mechanical equilibrium equation of $\partial\sigma_{ij}/\partial x_j=0$, $i=1,2,3$. The last term in Eq. (2) is the self-electrostatic energy density, which is expressed as $f_{\text{elec}}=-\frac{1}{2}E_iP_i$,[10] where E_i is the component of the electric field vector along the x_i direction. The self-electrostatic field is the negative gradient of the electrostatic potential, i.e., $E_i=-\partial\phi/\partial x_i$.

We use lead titanate (PT) thin layers as an example for numerical simulations. We solve the TDGL Eq. (1) using the semi-implicit Fourier-spectral method.[23] The material constants for the Landau free energy and the electrostrictive coefficients in the simulations are taken from Refs. 8 and 24: $\alpha_1=3.8(T-479)\times10^5$, $\alpha_{11}=-7.2\times10^7$, $\alpha_{12}=7.5\times10^8$, $\alpha_{111}=2.6\times10^8$, $\alpha_{112}=6.1\times10^8$, $\alpha_{123}=-3.7\times10^9$, $Q_{11}=0.089$, $Q_{12}=-0.026$, $Q_{44}=-0.033\,75$, $c_{11}=1.776\times10^{11}$, $c_{12}=9.636\times10^{10}$, and $c_{44}=1.220\times10^{11}$. All the parameters are in the International System of units except the unit of temperature T, which is in °C. In the computer simulations, we use normalized materials constants, which are the same as those in Ref. 13. The normalized gradient coefficients are $G_{11}/G_{110}=0.6$, $G_{12}/G_{110}=0.0$, and $G_{44}/G_{110}=G'_{44}/G_{110}=0.3$. A model size of $128\Delta x\times128\Delta x\times32\Delta x$ is employed, and periodic boundary conditions are applied along the x_1, x_2, and x_3 axes; Δx is the grid spacing. The grid spacing in real space is chosen as $\Delta x/l_0=1$, where $l_0=\sqrt{G_{110}/\alpha_0}$ and $\alpha_0=|\alpha_1|_{T=25\,^\circ\text{C}}$. The time step is $\Delta t/t_0=0.06$, where $t_0=1/\alpha_0L$. The thickness of the ferroelectric layer is taken as $h_f=16\Delta x$. The upper nonferroelectric layer thickness is the same as the lower thickness of $h_s=16\Delta x$.

We introduce the following notations for the different equilibrium domain structures that may occur in the ferroelectric layers: (i) *a*-type domain structure, where $\mathbf{P}=(P_1,0,0)$; (ii) *b*-type domain structure, where $\mathbf{P}=(0,P_2,0)$; (iii) *c*-type domain structure, where $\mathbf{P}=(0,0,P_3)$; (iv) *ab*-type domain structure, where $\mathbf{P}=(P_1,(_2,0)$; (v) *ac*-type domain structure, where $\mathbf{P}=(P_1,0,P_3)$ (vi) *bc*-type domain structure, where $\mathbf{P}=(0,P_2,P_3)$; and (vii) *abc*-type domain structure, where either $\mathbf{P}=(P_1,P_2,P_3)$. Figure 1 shows the misfit strain-misfit strain phase diagram for the epitaxial PT layer at room temperature, indicating that seven types of the domain structures exist in the misfit strain-misfit strain phase diagram for misfit strains ranging from −0.02 to 0.02. The *a*- and *b*-type domain structures appear only in the regions where the unequally biaxial misfit strains are tensile in one direction and compressive in another direction. The *c*-type domain structures exist when the misfit strains are compressive in both directions, whereas the *ab*-type domain structures only exist when the misfit strains are tensile in both directions. For the PT layers, the unequally biaxial misfit strains with one tensile and one compressive components are necessary for the formation of the *a*-type or *b*-type domain structures, which are forbidden when the misfit strains are equally biaxial, thereby suggesting that the unequally biaxial misfit strains must be imposed on the ferroelectric layers by their substrates in order to obtain the stable and desirable in-plane tetragonal phases.

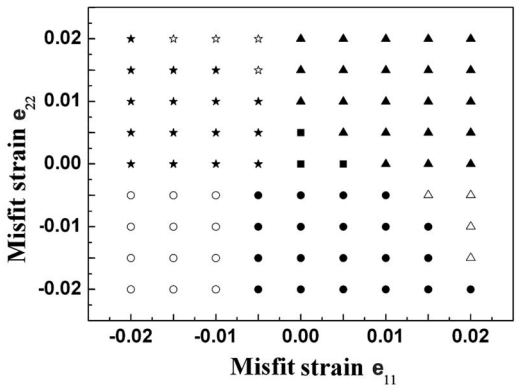

FIG. 1. Misfit strain-misfit strain phase diagram of the PT thin layer at room temperature, where symbol △ denotes *a*-type domain structure, symbol ☆ denotes *b*-type domain structure, symbol ◯ denotes *c*-type domain structure, symbol ▲ denotes *ab*-type domain structure, symbol ★ denotes *bc*-type domain structure, symbol ● denotes *ac*-type domain structure, and symbol ■ denotes *abc*-type domain structure.

Figures 2(a)–2(g) show the details of the polarization domain structures, which correspond to the phases shown in the phase diagram in Fig. 1. Figure 2(a) illustrates the domain structure when $e_{11}=0.02$ and $e_{22}=-0.005$. One can find that *a*-type domain structure has a multidomain structure, where *a*+ and *a*− domains exist with 180° domain walls between them. Figure 2(b) indicates the domain structure in *b*-type domain structure when $e_{11}=-0.01$ and $e_{22}=0.02$. The multidomain structure of *b*-type domain structure is slightly different from that in *a*-type domain structure. Some *b*-domains do not go the entire thickness of the layer, as shown in Fig. 2(b). More investigations are under progress to understand this phenomenon. Figure 2(c) illustrates the domain structure in *c*-type domain structure when $e_{11}=-0.02$ and $e_{22}=-0.02$. Comparing Fig. 2(c) with Fig. 2(a) or Fig. 2(b) indicates that the out-plane *c*-type domain structure has a more complex domain structure than the in-plane *a* or *b* domain structure. Figure 2(d) illustrates the domain structure in *ab*-type domain structure when $e_{11}=0.015$ and $e_{22}=0.0$ in

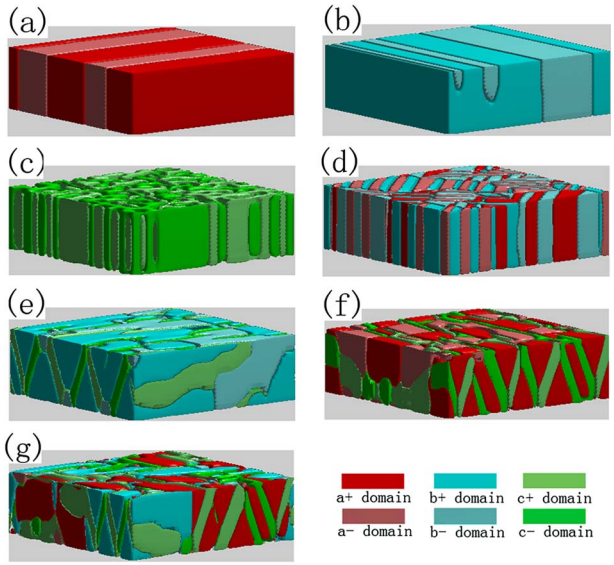

FIG. 2. (Color online) Polarization domain structures of the phases.

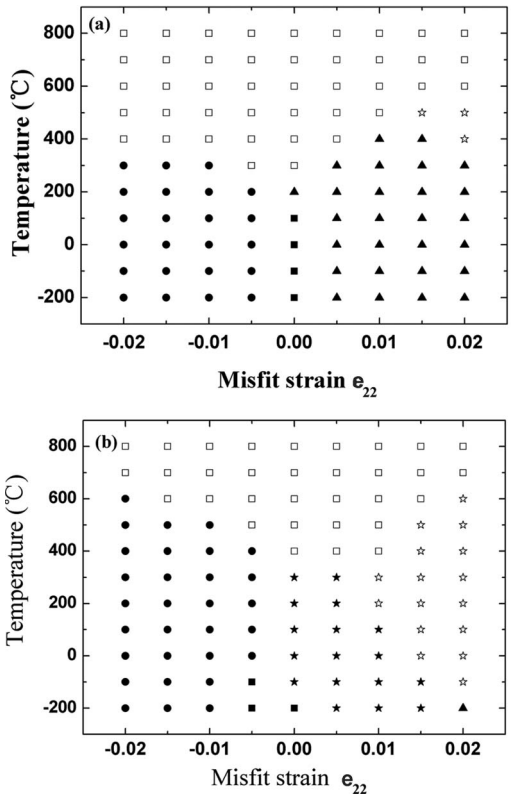

FIG. 3. Temperature-misfit phase diagrams at the constant misfit strains of $e_{11}=0.005$ (a) and $e_{11}=-0.005$ (b) of the PT thin layers, where symbol □ denotes the paraelectric phase and other symbols have the same meaning as that used in Fig. 1.

which the volume fractions of the *a* and *b* domains are 84% and 16%, respectively. In addition to 180° domain walls, 90° domain walls appear in this case. Figure 2(e) shows the domain structure in *bc*-type domain structure when $e_{11}=-0.02$ and $e_{22}=0.015$. In this case, the volume fractions of the *b* and *c* domains are 66% and 34%, respectively. Similarly, Figs. 2(f) and 2(g) denote the domain structures in *ac*-type domain structure when $e_{11}=0.01$ and $e_{22}=-0.02$ and in *abc*-type domain structure when $e_{11}=0.0$ and $e_{22}=0.0$. In Fig. 2(f), the volume fractions of *a* and *c* domains are 57% and 43%, respectively, whereas the volume fractions of *a*, *b*, and *c* domains are 34%, 28%, and 38%, respectively, in Fig. 2(g). These results indicate that the domain structures and volume fractions of different domains depend highly on the misfit strains of e_{11} and e_{22} at a given temperature.

Figures 3(a) and 3(b) show two-dimensional "temperature-strain" phase diagrams for the PT layer with $e_{11}=0.005$ and $e_{11}=-0.005$, respectively, when e_{22} changes from −0.02 to 0.02. Due to the unequally biaxial misfit strains, the paraelectric-to-ferroelectric transition boundaries for the PT layer have plateaus below the paraelectric phase for both cases, which is different from the "seagull" shape of the transition temperature versus the equally biaxial misfit strain.[8] The significant feature induced by the unequally biaxial misfit strains is the formation of the tetragonal ferroelectric phase, which does not exist in the PT film under equally biaxial misfit strains.[8] In the temperature-misfit phase diagrams, at the constant misfit strain of $e_{11}=0.005$, only four domains exist: (i) the *b* domain, (ii) the *ab* domain, (iii) the *ac* domain, and (iv) the *abc* domain. At the same time, the *ab* and *ac* domains may occupy a large region in the total domain diagram. However, at the constant misfit strain of $e_{11}=-0.005$, there exist five domains: (i) the *b* domain, (ii) the *ab* domain, (iii) the *ac* domain, (iv) the *bc* domain, and (v) the *abc* domain. Among the five domains, the *ac* and *b* domains may occupy a large region in the total domain diagram. Thus, compared with $e_{11}=0.005$, the misfit strain of $e_{11}=-0.005$ favors the formation of *b* domains.

In summary, the phase diagrams and the equilibrium domain structures of PT ferroelectric thin layers under unequally biaxial misfit strains have been studied by using three-dimensional phase field simulations. The polarization gradient energy (domain wall energy) and the long-range mechanical and electrostatic interactions are all taken into account, which are usually excluded in thermodynamics calculations based on a single-domain assumption. It is found that unequally biaxial misfit strains lead to the presence of a single tetragonal variant under highly anisotropic substrate strains.

This work was supported by the National Natural Science Foundation of China under Grant Nos. 50572006, 50632010, 50571011, and 50428101, the HKUST Fok Ying Tung Graduate School under Project No. NRC06/07.EG04, and (U.S.) Department of Energy under Grant No. DE-FG02-07ER46417.

[1] M. J. Dalberth, R. E. Stauber, J. C. Price, C. T. Roger, and D. Galt, Appl. Phys. Lett. **72**, 507 (1998).
[2] Q. X. Jia, A. T. Findikoglu, D. Reagor, and P. Lu, Appl. Phys. Lett. **73**, 897 (1998).
[3] H. N. Lee, D. Hesse, N. Zakharov, and U. Gosele, Science **296**, 2006 (2002).
[4] C. H. Ahn, K. M. Rabe, and J. M. Triscone, Science **303**, 488 (2004).
[5] C. L. Chen, H. H. Heng, Z. Zhang, A. Brazdeikis, Z. J. Huang, W. K. Chu, C. W. Chu, F. A. Miranda, F. W. Van Keuls, R. R. Romanofsky, and Y. Liou, Appl. Phys. Lett. **75**, 412 (1999).
[6] J. S. Speck and W. Pompe, J. Appl. Phys. **76**, 466 (1994).
[7] S. P. Alpay and A. L. Roytburd, J. Appl. Phys. **83**, 4714 (1998).
[8] N. A. Pertsev, A. G. Zembilgotov, and A. K. Tagantsev, Phys. Rev. Lett. **80**, 1988 (1998).
[9] V. G. Koukhar, N. A. Pertsev, and R. Waser, Phys. Rev. B **64**, 214103 (2001).
[10] Y. L. Li, S. Y. Hu, Z. K. Liu, and L. Q. Chen, Appl. Phys. Lett. **81**, 427 (2002).
[11] J. Wang and T. Y. Zhang, Appl. Phys. Lett. **86**, 192905 (2005).
[12] S. Hoon Oh and H. M. Jang, Phys. Rev. B **62**, 14757 (2000).
[13] Y. L. Li, S. Y. Hu, Z. K. Liu, and L. Q. Chen, Acta Mater. **50**, 395 (2002).
[14] Y. Lin, X. Chen, S. W. Liu, C. L. Chen, J. S. Lee, Y. Li, Q. X. Jia, and A. Bhalla, Appl. Phys. Lett. **84**, 577 (2004).
[15] H. N. Lee and D. Hesse, Appl. Phys. Lett. **80**, 1040 (2002).
[16] A. Garg, Z. H. Barber, M. Dawber, J. F. Scott, A. Snedden, and P. Lightfoot, Appl. Phys. Lett. **83**, 2414 (2003).
[17] J. H. Qiu and Q. Jiang, J. Appl. Phys. **101**, 034110 (2007).
[18] Y. M. Tao and Y. Z. Wu, J. Appl. Phys. **101**, 024111 (2007).
[19] H. X. Cao, V. C. Lo, and Z. Y. Li, J. Appl. Phys. **101**, 014113 (2007).
[20] K. Binder, Ferroelectrics **35**, 99 (1981).
[21] D. R. Tilley and B. Zeks, Solid State Commun. **108**, 147 (1998).
[22] A. F. Devonshire, Philos. Mag., Suppl. **3**, 85 (1954).
[23] L. Q. Chen and J. Shen, Comput. Phys. Commun. **108**, 147 (1998).
[24] M. J. Haun, E. Furman, S. J. Jang, H. A. Mckinstry, and L. E. Cross, J. Appl. Phys. **62**, 3331 (1987).